EurJOC
European Journal of Organic Chemistry

Research Article
doi.org/10.1002/ejoc.202200111

Chemistry Europe
European Chemical Societies Publishing

www.eurjoc.org

Special Collection

^{113}Cd as a Probe in NMR Studies of Allosteric Host-Guest-Ligand Complexes of Porphyrin Cage Compounds

Jeroen P. J. Bruekers,[a] Matthijs A. Hellinghuizen,[a] Anne Swartjes,[a] Paul Tinnemans,[a] Paul B. White,[a] Johannes A. A. W. Elemans,*[a] and Roeland J. M. Nolte*[a]

Cadmium porphyrin cage compounds **Cd1** and **^{113}Cd1** have been synthesized from the free base porphyrin cage derivative **$H_2$1** and $Cd(OAc)_2 \cdot 2\ H_2O$ or $^{113}Cd(OAc)_2 \cdot 2\ H_2O$, respectively. The compounds form allosteric complexes with the positively charged guests *N,N′*-dimethylimidazolium hexafluorophosphate (**DMI**) and *N,N′*-dimethylviologen dihexafluorophosphate (**Me_2V**), which bind in the cavity of the cage, and **tbupy**, which coordinates as an axial ligand to the outside of the cage. In the presence of **tbupy**, the binding of **DMI** in **Cd1** is enhanced by a factor of ~31, while the presence of **DMI** or **Me_2V** in the cavity of **Cd1** enhances the binding of **tbupy** by factors of 55 and 85, respectively. The X-ray structures of the coordination complexes of **Cd1** with acetone, acetonitrile, and pyridine, the host-guest complex of **Cd1** with a bound viologen guest, and the ternary allosteric complex of **Cd1** with a bound **DMI** guest and a coordinated **tbupy** ligand, were solved. These structures revealed relocations of the cadmium center in and out of the porphyrin plane, depending on whether a guest or a ligand is present. ^{113}Cd NMR could be employed as a tool to quantify the binding of guests and ligands to **^{113}Cd1**. 1D EXSY experiments on the ternary allosteric system **Cd1-tbupy-Me_2V** revealed that the coordination of **tbupy** significantly slowed down the dissociation of the **Me_2V** guest. Eyring plots of the dissociation process revealed that this kinetic allosteric effect is entropic in nature.

Introduction

As part of a program aimed at the development of processive catalysts capable of writing binary information on polymer chains,[1,2] we intend to develop tools to closely study the working mechanisms of these systems. The catalysts are based on porphyrin cage compounds of the type depicted in Figure 1, and exhibit allosteric binding properties when a zinc center is present in the porphyrin (**Zn1**). The binding of *N,N′*-dimethylviologen dihexafluorophosphate (**Me_2V**) in the cavity of this host is enhanced by a factor of 75 when the axial ligand 4-*tert*-butylpyridine (**tbupy**) is coordinated to the zinc center at the outside of the cage and the coordination of **tbupy** is enhanced by a factor 72 when **Me_2V** is present at its inside.[3] The manganese derivative of the porphyrin cage (**Mn1**) has been employed as a processive epoxidation catalyst capable of efficiently converting a polyalkene into a polyepoxide.[4,5]

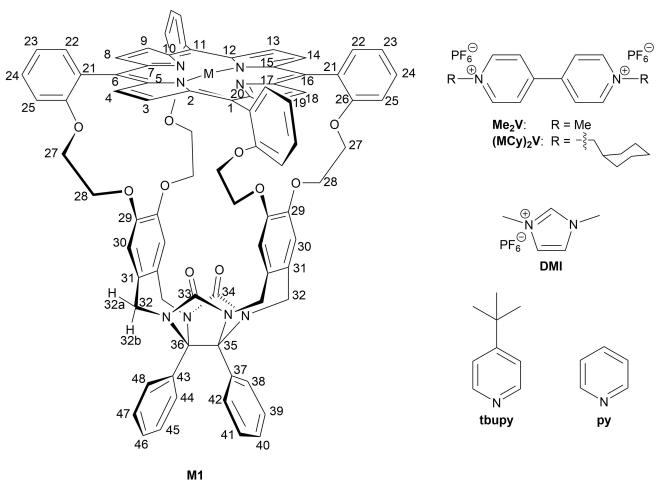

Figure 1. Structure of porphyrin cages **M1** (M = 2H, Zn, MnCl, Cd, ^{113}Cd) with the used atom labeling, and structures of guests **Me_2V**, **$(MCy)_2$V** and **DMI**, and ligands **tbupy** and **py**.

Several other porphyrin cage derivatives with allosteric binding properties have been reported,[1,6–10] and in these studies it was reasoned that the coordination geometry at the porphyrin metal played a vital role in the allosteric behavior. Electrostatic repulsion between a bound dicationic **Me_2V** guest and the metal center was proposed to structurally relocate the latter in a direction away from the cage, i.e., to the outside of the porphyrin ring, thereby making it better available for coordination of the **tbupy** ligand. Analogously, the initial coordination of the ligand would pull the metal to the outside of the porphyrin plane, thereby creating more possibilities (both in terms of

[a] *J. P. J. Bruekers, M. A. Hellinghuizen, A. Swartjes, Dr. P. Tinnemans, Dr. P. B. White, Dr. J. A. A. W. Elemans, Prof. Dr. R. J. M. Nolte*
Radboud University, Institute for Molecules and Materials,
Heyendaalseweg 135, 6525AJ, Nijmegen, The Netherlands
E-mail: J.Elemans@science.ru.nl
R.Nolte@science.ru.nl
www.ru.nl/science/molecularnanotechnology

Supporting information for this article is available on the WWW under https://doi.org/10.1002/ejoc.202200111

Special Collection *Part of a joint Special Collection with ChemCatChem and EurJOC on the Netherlands Institute for Catalysis Research. Please click here for more articles in the collection.*

sterics and electrostatic repulsion) for **Me_2V** to bind inside the cavity. So far, however, predominantly circumstantial evidence for these hypotheses has been found. In order to investigate the role of the metal center in the allosteric binding properties of these porphyrin cages in more detail, we have inserted an NMR-active cadmium center into the porphyrin. Already for more than 40 years, ^{113}Cd has been used to study the interactions of metal centers in proteins.[11–15] ^{113}Cd *meso*-tetraphenylporphyrins (**^{113}CdTPP**) have been the subject of research in the early years of ^{113}Cd NMR spectroscopy.[16–18] More recently, studies of metal-migration processes in allosteric Newton's cradle-like molecular devices[17] made use of ^{113}Cd centers to identify their coordinative interactions with a porphyrin with the help of ^{113}Cd NMR spectroscopy.[19]

In an effort to elucidate the role of the metal center in cooperative/allosteric systems based on porphyrin cages **Zn1** and **Mn1**, we have inserted cadmium centers from naturally abundant and enriched ^{113}Cd sources into the porphyrin ring of **$H_2$1**. With the help of ^{1}H and ^{113}Cd NMR spectroscopy, we have investigated the allosteric binding properties between **Cd1**, **tbupy**, and the dicationic guest **Me_2V**, and those between **Cd1**, **tbupy**, and the monocationic guest *N*,*N*′-dimethylimidazolium hexafluorophosphate (**DMI**). We have been able to solve several crystal structures of complexes of **Cd1**, amongst which that of the allosteric ternary complex between **Cd1**, **tbupy**, and **DMI**.

Results and Discussion

Synthesis

$^{113}Cd(OAc)_2\cdot 2H_2O$ was prepared by dissolving ^{113}CdO (~90% enriched in ^{113}Cd) in boiling acetic acid,[20] followed by precipitation in diethyl ether (yield 89%). Porphyrin cage compounds **Cd1** and **^{113}Cd1** and reference compound **CdTPP** were prepared from **$H_2$1** or **H_2TPP** and $Cd(OAc)_2\cdot 2H_2O$ or $^{113}Cd(OAc)_2\cdot 2H_2O$ by heating the components at reflux in a 1:2 (v/v) solvent mixture of methanol and chloroform, to give the products as green powders (90%, 77%, 67% yield, respectively) after purification by column chromatography and precipitation. The ^{1}H NMR spectrum of **Cd1** shows a $^4J_{H-Cd}$-coupling of ~6 Hz between the β-pyrrole protons and the ^{113}Cd center of the porphyrin. In contrast to the ^{1}H NMR spectra of **CdTPP** (Figure S4.97), the spectra of **Cd1** and **^{113}Cd1** in chloroform were found to be concentration-dependent (Figure 2A, Figure 2B). Most notably, the signals of the *ortho*-protons of the phenyl groups of the diphenylglycoluril scaffold (*H*-38, *H*-42, *H*-44, *H*-48), the sidewall protons (*H*-30) and the benzylic protons (*H*-32a,b), in the ^{1}H NMR spectra, as well as the signal of the cadmium center in the ^{113}Cd spectra, shifted upfield considerably at increasing concentration of the compounds. These shifts suggest that the cadmium porphyrin cages aggregate in solution. At their limit of solubility (~5 mM), this aggregation was not yet complete since the addition of more **Cd1** still

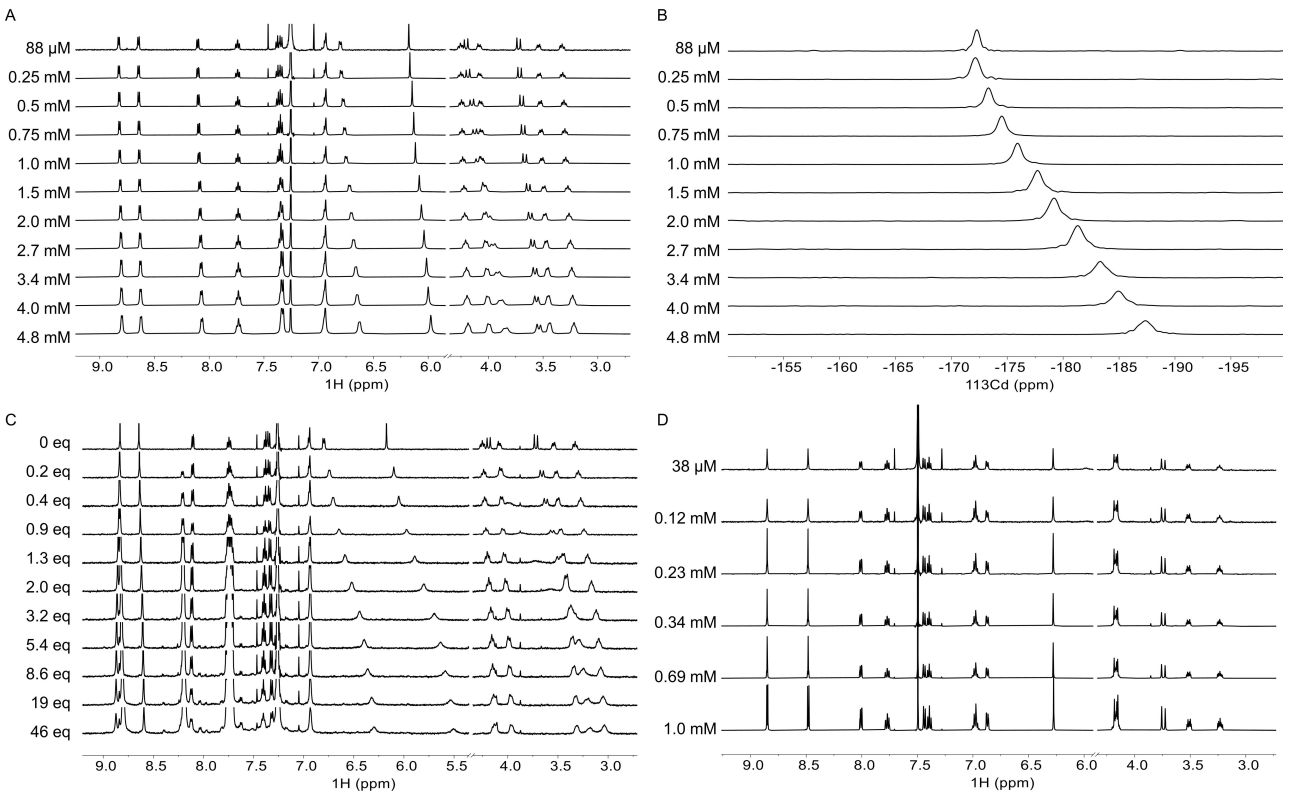

Figure 2. (A) ^{1}H NMR (500 MHz, $CDCl_3$, 298 K) and (B) ^{113}Cd NMR (111 MHz, $CDCl_3$, 298 K) spectra extracted from non-uniform sampled ^{1}H–^{113}Cd HMBC spectra of **^{113}Cd1** at various concentrations. (C) ^{1}H NMR spectra (500 MHz, $CDCl_3$, 298 K) spectra of a titration of **Cd1** (c = 0.22 mM) with **CdTPP**. (D) ^{1}H NMR spectra (500 MHz, $CDCl_3/CD_3CN$, 1:1, v/v, 298 K) of **Cd1** at various concentrations.

caused changes in chemical shift. Analogous to zinc porphyrins, cadmium porphyrins easily attract an axial ligand. In the case of **Cd1**, the urea carbonyl oxygen atoms likely coordinate to the cadmium atom of another molecule of **Cd1** (see Figures S6.1 and S6.2 for a molecular model), causing the aforementioned protons close to these carbonyl groups to shift upfield at increasing concentrations of **Cd1**, as a result of shielding by the strong ring current of the porphyrin. These chemical shifts could be fitted most accurately to a dimerization model in which it was assumed that no cooperativity exists between subsequent binding events (isodesmic assembly), resulting in $K_{dimer} = 67\ M^{-1}$. Due to competition with this self-coordination process, all measured K_a-values of the coordination of externally added axial ligands to the Cd center of the cage will be apparent ones.

To further investigate the role of the diphenylglycoluril part of the cage in this aggregation process, a ^{1}H NMR titration was performed in which **CdTPP** (0 to 46 equivalents) was added to **Cd1** ($c = 0.217$ mM) in $CDCl_3$ (Table 1). Upon the addition of **CdTPP** similar chemical shift changes were observed for the protons of **Cd1** as in the previous experiment (Figure 2A, Figure 2C). The titration curve could be fitted both to a 1:1 binding equilibrium, giving $K_a = 3.91 \pm 0.16 \times 10^3\ M^{-1}$, and to a 1:2 binding event (assuming non-cooperative binding), $K_1 = 6.26 \pm 0.01 \times 10^3\ M^{-1}$ and $K_2 = 1.57 \pm 0.01 \times 10^3\ M^{-1}$. Hence, the curve fittings provided no clear conclusion as to whether one or two **CdTPP** molecules bind to **Cd1**, but the magnitude of the K_a-values indicates that **CdTPP** coordinates to **Cd1** with considerable strength. The difference in association constant between binding to a **CdTPP** or to another **Cd1** molecule could be due to the higher degree of flexibility of the porphyrin plane of **CdTPP** compared to the porphyrin plane of the fairly rigid **Cd1**, but it is more likely that a residual solvent or water molecule is coordinated to the cadmium center inside the cavity of **Cd1**, reducing its affinity for an additional axial ligand, i.e., the urea carbonyl groups of **Cd1**.

Solvent effects

When **Cd1** was dissolved in $CDCl_3/CD_3CN$ (1:1, v/v) (Figure 2D) or DMSO-d_6 (Figure S4.14), no signs of aggregation were observed up to the maximum solubility of the compound (~ 1 mM and ~11 mM, respectively), indicating that coordination of the solvent outcompetes coordinative self-association of **Cd1**. From an ^{1}H NMR titration between **Cd1** and MeCN in $CDCl_3$, an association constant $K_a = 17\ M^{-1}$ (Table 1) was calculated. This significant binding strength of acetonitrile gives rise to competition with the coordination of pyridine derivatives to **Cd1** (*vide infra*).

Binding properties

Prior to employing ^{113}Cd NMR to investigate the allosteric behavior of **Cd1** with viologen guests and axial ligands, the binding properties of the individual guests and ligands were established. First, the binding of **Me_2V** in the cavity of **Cd1** was investigated with the help of UV-vis titrations (Table 1). The obtained titration curves indicated very strong binding of the guest ($K_a > 10^7\ M^{-1}$), but because of this the binding strengths could not be reliably determined with the standard fitting methods (Figure S5.1). Therefore, **DMI** was used as an alternative guest to investigate allosteric behavior. Since this guest

Table 1. Association constants between **Cd1** and various guests or ligands.

Entry	Host concentration [μM]	Guest or ligand	Additive	Additive concentration [M]	Initial fractional saturation of **Cd1** by the additive	Apparent association constant K_a [M^{-1}]
1[a,c]	$88-4.8\times10^3$	**Cd1**	–	–	–	67 ± 36
2[a,c,h]	217	**CdTPP**	–	–	–	$3.91 \pm 0.16 \times 10^3$
3[a,c,i]	217	**CdTPP**	–	–	–	$6.26 \pm 0.01 \times 10^3$
4[a,c]	892	MeCN	–	–	–	$1.68 \pm 0.05 \times 10^1$
5[d,e,f]	0.496	**Me_2V**	–	–	–	$> 10^7$
6[b,c]	2.07	**py**	–	–	–	$3.97 \pm 0.18 \times 10^5$
7[b,d]	2.07	**py**	–	–	–	$9.11 \pm 3.16 \times 10^3$
8[a,g]	4.1×10^3	**py**	–	–	–	4.17 ± 0.06
9[a,c]	822	**tbupy**	–	–	–	$1.01 \pm 0.90 \times 10^3$
10[a,d]	869	**tbupy**	–	–	–	23 ± 11
11[a,d]	849	**tbupy**	**Me_2V**	0.00186	> 0.99	$1.97 \pm 0.02 \times 10^3$
12[a,d]	656	**tbupy**	**DMI**	0.000667	0.32	$2.39 \pm 0.01 \times 10^2$
13[a,d]	819	**tbupy**	**DMI**	0.00200	0.59	$5.26 \pm 0.04 \times 10^2$
14[a,d]	690	**tbupy**	**DMI**	0.00671	0.83	$1.11 \pm 0.04 \times 10^3$
15[a,d]	905	**tbupy**	**DMI**	0.0175	0.93	$1.34 \pm 0.03 \times 10^3$
16[b,d]	2.01	**DMI**	–	–	–	$2.83 \pm 0.48 \times 10^3$
17[b,d]	1.92	**DMI**	**tbupy**	0.00621	0.04	$7.31 \pm 0.32 \times 10^3$
18[b,d]	2.09	**DMI**	**tbupy**	0.0340	0.17	$1.88 \pm 0.30 \times 10^4$
19[b,d]	2.10	**DMI**	**tbupy**	0.0676	0.29	$4.02 \pm 0.41 \times 10^4$
20[b,d]	1.83	**DMI**	**tbupy**	0.621	0.79	$6.58 \pm 0.18 \times 10^4$

[a] Determined by ^{1}H NMR titrations in duplo. [b] Determined by UV-Vis titrations in triplo [c] In $CHCl_3$ or $CDCl_3$. [d] In $CHCl_3/CH_3CN$ (1:1, v/v) or $CDCl_3/CD_3CN$ (1:1, v/v). [e] Poor titration curve fits were obtained. [f] Determined by UV-Vis titrations in duplo. [g] In DMSO-d_6. [h] Fitted to a 1:1 binding equilibrium. [i] Fitted to a non-cooperative 1:2 binding equilibrium; K_1 is reported, $K_2 = K_1/4$.

Table 2. Selected ^{1}H and ^{113}Cd NMR chemical shifts of host/guest/ligand systems in various solvents.

Entry	Ligand or guest	Concentration of ligand or guest [mM]	Chemical shift [ppm] δ ^{113}Cd	^{1}H δ *H*-3,4,13,14	δ *H*-8,9,18,19	δ *H*-22	δ *H*-30	δ *H*-27b	δ *H*-27a	δ *H*-28b	δ *H*-28a
1	–[a,d]	–	−171.57	8.83	8.65	8.11	6.19	4.26	4.08	3.55	3.33
2	–[a,e]	–	−174.37	8.82	8.64	8.09	6.11	4.23	4.05	3.51	3.29
3	–[b,e]	–	−247.82	8.85	8.48	8.01	6.27	4.17	4.17	3.51	3.23
4	–[c,f]	–	−260.43	8.76	8.40	7.92	6.29	4.24	4.24	3.45	3.21
5	**tbupy**[a,e]	8.9	−200.88	8.59	8.68	8.13	6.19	4.06	3.79	3.42	3.23
6	**py**[a,e]	8.6	−201.89	8.89	8.51	8.16	6.03	3.90	3.82	3.02	2.64
7	**tbupy**[b,e]	325	−221.15	8.76	8.54	8.09	6.17	4.02	3.92	3.35	2.98
8	**py**[b,e]	8.8	−211.00	8.87	8.46	8.12	6.03	3.89	3.83	3.13	2.65
9	**DMI**[b,e]	10.3	−246.26	8.78	8.67	8.08	6.12	4.21	4.21	3.66	3.25
10	**Me_2V**[b,e]	2.1	−254.71	8.96	8.69	8.21	5.96	3.97	3.97	3.36	2.47
11	**tbupy**, **DMI**[b,e]	11.2 10.2	−225.78	8.75	8.71	8.03	6.12	4.21	4.21	3.67	3.25
12	**tbupy**, **Me_2V**[b,e]	11.2 2.1	−234.33	8.95	8.68	8.12	5.97	3.98	3.98	3.37	2.50

[a] In $CDCl_3$. [b] In $CDCl_3/CD_3CN$ (1:1, v/v). [c] In DMSO-d_6. [d] [^{113}**Cd1**] = 8 μM. [e] [^{113}**Cd1**] = 1.0 mM. [f] [^{113}**Cd1**] = 8.2 mM.

carries only one positive charge and has a smaller π-system than **Me_2V**, a lower binding strength with **Cd1** was expected. UV-vis titrations of the binding process indeed yielded reliable fits of the titration curves, and the binding constant between **DMI** and **Cd1** was determined to be $K_a = 2.83 \times 10^3\ M^{-1}$ (Table 2; *vide infra* for a detailed NMR characterization of the **DMI**-**Cd1** complex).

In the next series of experiments, the coordination of pyridine ligands to the Cd center of **Cd1** was investigated (Table 1). The association constants of **Cd1** with **tbupy**, determined by ^{1}H NMR spectroscopy, and with pyridine (**py**), determined by UV-vis spectroscopy, in chloroform were $K_a = 1.01 \times 10^3\ M^{-1}$ and $K_a = 3.97 \times 10^5\ M^{-1}$, respectively. The stronger binding of **py** is the result of its coordination inside the cavity of **Cd1**, where it experiences additional favorable π-π stacking interactions with the cavity sidewalls and a cavity filling effect.[21] Interestingly, the Soret band of **Cd1** in chloroform is quite broad (Figure S5.31) with a lower intensity compared to the Soret band of **Cd1** in $CHCl_3$/MeCN (1:1, v/v) (Figure S5.34). The addition of **py** to the solution of **Cd1** in chloroform caused the Soret band to sharpen to a similar shape as that observed in $CHCl_3$/MeCN (1:1, v/v) in the absence of **py**. We attribute the initial broad shape of the Soret band to a poorly defined axial coordination of e.g. residual water or methanol molecules, and the subsequent sharpening of the signal to the stronger coordination of **py** or MeCN, resulting in the formation of better-defined **Cd1**-ligand complexes. Compared to their coordination in chloroform, the binding strengths of **Cd1** with **tbupy** and **py** in $CHCl_3$/MeCN (1:1, v/v) dropped significantly with a factor of ~44 to $K_a = 23\ M^{-1}$ and $9.11 \times 10^3\ M^{-1}$ (Table 1), respectively, corresponding in both cases to a $\Delta\Delta G_{binding}$ of $\sim +9\ kJ\,mol^{-1}$. The binding strength of acetonitrile to **Cd1** in $CDCl_3$ with $K_a = 17\ M^{-1}$, equaling an energy of $\Delta G_{binding} = -7.0\ kJ\,mol^{-1}\ K^{-1}$, is close to the abovementioned competitive binding free energy value. Competition of the solvent for ligand coordination is even more prominent in DMSO-d_6, in which the association constant between **py** and **Cd1** dropped to a value of $K_a = 4\ M^{-1}$ (Table 1).

The interplay between **DMI** guest binding and **tbupy** ligand coordination to **Cd1** was investigated in a next series of titration experiments. Previously, we reported binding equations that described a similar interplay between viologen guest binding and **tbupy** coordination to the related porphyrin cage **Zn1** (see Supplementary Information).[3]

The parameter describing this interplay is the fractional saturation y_{R-G}, defined as the fraction of receptor molecules R occupied by a guest or ligand G. In the case of ligands that coordinate to the metal center of **Cd1**, this y_{R-G} value was calculated by employing equations 1–11 in the Supporting Information to account for coordinative solvent competition. $^{A}K_B$ is the association constant of ligand/guest B at full receptor saturation by ligand/guest A, and $^{A}K_{B\text{-}app}$ is the apparent association constant of ligand/guest B at a particular fractional saturation of the receptor by guest/ligand A. To obtain the values of $^{tbupy}K_{DMI}$ and $^{DMI}K_{tbupy}$, the apparent *K*-values of the binding of component B need to be determined at various fractional saturations of the receptor by additive A. A linear relationship should be obtained when these apparent association constants are plotted as a function of the fractional saturation. To this end, the titrations with either **DMI** (Table 1, Figure 3A) or **tbupy** (Table 1, Figure 3B) were repeated, but now in the presence of variable amounts of the other component.

The binding experiments show that an increase in the fractional saturation of **Cd1** by either **DMI** or **tbupy** leads to a significant increase in the apparent association constant of the other coordinating or binding component, respectively **tbupy** or **DMI**. When a straight line was fitted through the obtained apparent values, the value of the association constant of **DMI** that can be expected at full occupancy of **Cd1** by **tbupy** could be extrapolated: $^{tbupy}K_{DMI} = 8.9 \times 10^4\ M^{-1}$. Compared to the binding between **Cd1** and **DMI** in the absence of **tbupy**, the allosteric magnification factor by which the association constant is increased amounts to 31. Analogously, for the coordination of **tbupy** to **Cd1** the extrapolated value for the association constant at full occupancy of **Cd1** by **DMI** is $^{DMI}K_{tbupy} = 1.3 \times$

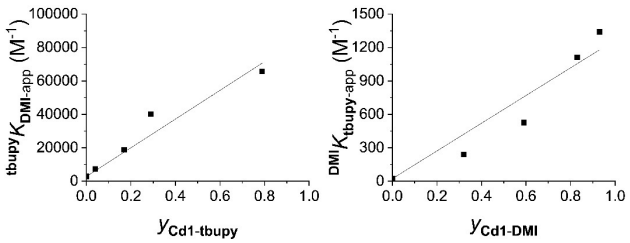

Figure 3. Apparent association constants between **Cd1** and (A) **DMI** and (B) **tbupy** plotted as a function of the occupancy (fraction of host occupied with an additive) at the start of the titration by (A) **tbupy** and (B) **DMI**. Linear fitting of the data in (A) yields the equation ${}^{tbupy}K_{DMI\text{-}app} = (85931 \pm 7850) * y_{Cd1\text{-}tbupy} + 2830$ with $R^2 = 0.928$. Fitting the data in (B) yields the equation ${}^{DMI}K_{tbupy\text{-}app} = (1244 \pm 120) * y_{Cd1\text{-}DMI} + 23$ with $R^2 = 0.957$.

$10^3\ M^{-1}$, which amounts to an allosteric magnification factor of 55.

The allosteric magnification factor for the binding of **tbupy** to **Cd1** in the presence of **Me_2V** is even more prominent, i.e., 77 or 85, depending on whether the value was determined by a ^{1}H or ^{113}Cd NMR titration, respectively. This factor is also slightly larger than the factor of 72 found for the binding of **tbupy** to **Zn1** in the presence of **Me_2V**.[3] The ${}^{Me2V}K_{tbupy}$-value was determined by both ^{1}H and ^{113}Cd NMR titrations, resulting in ${}^{Me2V}K_{tbupy} = 1.76 \pm 0.04 \times 10^3\ M^{-1}$ and $1.97 \pm 0.02 \times 10^3\ M^{-1}$, respectively (Table S5.1). The similar values obtained for ${}^{Me2V}K_{tbupy}$ show that the ^{113}Cd signal is a reliable probe for determining the binding strength of an axial ligand to **Cd1**.

Structural studies by NMR

To investigate the effect of guest and ligand binding on the structure of **Cd1**, the ^{1}H NMR, ^{13}C NMR, and ^{113}Cd NMR spectra of a series of host-guest/ligand mixtures were recorded. In Table 2, the relevant chemical shifts of protons of **^{113}Cd1** in these complexes are summarized. A 125-fold variation in concentration of **Cd1** in $CDCl_3$ revealed that the host displays self-association (Table 2, Figure 2A, Figure 2B). It is estimated that at a concentration of 1.0 mM in $CDCl_3$, 11% of the molecules of **^{113}Cd1** are self-associated (probably in the form of dimers). The effect of coordinating solvents/ligands on the ^{1}H and ^{113}Cd chemical shifts of **^{113}Cd1** becomes apparent from Table 2, Entries 1–4. Compared to spectra in $CDCl_3$, spectra in coordinating solvents cause small shifts (up to 0.25 ppm) of the proton signals of **^{113}Cd1** in the ^{1}H NMR spectra, while the Cd signals in the ^{113}Cd spectra shift upfield quite dramatically, i.e., −86 ppm in DMSO-d_6 and −73 ppm in CD_3CN. These shifts are in line with the literature, showing similar NMR shifts for a cadmium porphyrin in the solid-state that goes from a square-planar geometry to a square-pyramidal geometry with an oxygen or nitrogen as the fifth ligand.[22] The addition of **tbupy** to **^{113}Cd1** in $CDCl_3$ causes no large shifts of the ^{1}H NMR signals of protons lining the cavity of **^{113}Cd1** (*H*-27, *H*-28, and *H*-30), whereas the addition of **py** to **^{113}Cd1** results in significant upfield shifts (up to −0.7 ppm) of these proton signals (Table 2, entries 5 and 6). Similar behavior was observed for these systems in $CDCl_3/CD_3CN$ (1:1, v/v) (Table 2, entries 7 and 8). The observed shifts indicate that **py** coordinates to the cadmium center at the inside of the cage of **^{113}Cd1**, whereas **tbupy** coordinates to the outside, which is also reflected in the 400 times larger association constant between **^{113}Cd1** and **py** (Table 1) as a result of stabilizing cavity effects. The difference in binding geometries is further confirmed by the crystal structures obtained for both complexes (*vide infra*, Figure 6). Due to the broadness of the observable signals of the bound **py** ligand (at $\delta = 5.06$ and 3.37 ppm) and the coalesced signals of the **tbupy** ligand in the ^{1}H NMR spectra of the complexes, no host-ligand ROE contacts were observed in the 2D ROESY spectra. Interestingly, the effect of the coordination of **tbupy** (~90% occupancy) and **py** (>99% occupancy) on the ^{113}Cd shift of **^{113}Cd1** in $CDCl_3$ is very similar ($\Delta\delta = -26$ and −27 ppm upfield, respectively) (Table 2), which indicates that the chemical shift of the ^{113}Cd center is not significantly influenced by the binding environment of the pyridine-derived ligand, while it is governed by a change towards a penta-coordinate system due to the binding of a pyridine-derived ligand.[22]

The binding of **DMI** in **^{113}Cd1** in $CDCl_3/CD_3CN$ (1:1, v/v) induces a slight upfield shift ($\Delta\delta = -0.07$ ppm) of the ^{1}H NMR signal of the β-pyrrole protons above the cavity portals (*H*-3,4,13,14), which is likely caused by their proximity to the methyl groups of the bound guest. The signal of the sidewall protons *H*-30 shifts upfield by −0.15 ppm as a result of shielding by the aromatic surface of the guest. The ^{113}Cd signal only shifts slightly upfield, which may result from a repositioning of the cadmium center, to which an acetonitrile molecule is likely still coordinated, in the porphyrin. From the observed shifts one can conclude that a binding geometry in which the aromatic ring of **DMI** is oriented in a coplanar fashion with respect to the cavity sidewalls is most likely (Figure 6D). The coalesced signals of the **DMI** guest in the host-guest mixtures remain quite broad during the NMR studies. Upon the binding of **DMI** in **^{113}Cd1**, all **DMI** proton signals of the guest shift upfield by up to −0.8 ppm compared to uncomplexed **DMI**, as a result of shielding by the cavity of **^{113}Cd1**. When **tbupy** coordinates to the **^{113}Cd1**−**DMI** complex, the ^{1}H NMR signals of **^{113}Cd1** shift only marginally, in contrast to its ^{113}Cd signal, which shifts significantly downfield by +20.5 ppm. The coalesced proton signals of free and bound **DMI** shift upfield by ~−0.7 ppm compared to the shifts of the **Cd1**−**DMI** complex at the start of the **tbupy** titration (as a result of enhanced **DMI** binding inside the cavity) before broadening into the baseline. This broadening of the coalesced **DMI** signal indicates slower host-guest exchange rates than those in the absence of **tbupy**,[23] which suggests that the allosteric effect is both thermodynamic and kinetic (*vide infra*) in nature.

The binding of **Me_2V** in the cavity of **^{113}Cd1** in $CDCl_3/CD_3CN$ (1:1, v/v) has more pronounced effects on the structure of the host. The signals of the ethyleneoxy linker protons *H*-27 and *H*-28 and of sidewall proton *H*-30 shift upfield by up to −0.7 ppm, as a result of shielding by the aromatic surface of the guest. The proximity to the deshielding edge of the aromatic planes of **Me_2V** causes a downfield shift in the signal of the β-pyrrole

Research Article
doi.org/10.1002/ejoc.202200111

protons above the cavity portals. In contrast to the downfield shift observed for the cadmium NMR signal of **^{113}Cd1** upon the binding of **DMI**, the cadmium signal of **^{113}Cd1** shifts upfield by −7 ppm upon the binding of **Me_2V**, which may be caused by several factors or a combination thereof: (1) electrostatic repulsion between the cadmium center and the dicationic **Me_2V** molecule, (2) steric interactions between the cadmium center and the extended aromatic surfaces of the guest, and (3) relocation of a metal-coordinated axial ligand (most probably an acetonitrile molecule) from the inside to the outside of the cage. The addition of **tbupy** to this host-guest mixture does not result in significant changes in the ^{1}H NMR spectrum, similar to what was observed for the host-guest mixture of **^{113}Cd1** with **DMI**. Analogously, the cadmium signal of the **^{113}Cd1**−**Me_2V** complex shifts downfield by +20.5 ppm upon the coordination of **tbupy**. 1D ROESY experiments of the ternary complex **^{113}Cd1**−**Me_2V-tbupy** (Figure S4.98–S4.102) at −32 °C revealed ROE interactions between the **^{113}Cd1** host (β-pyrrole protons above the cavity portals *H*-3,4,13,14 and sidewall protons *H*-30) and the **Me_2V** guest (methyl protons and CH protons adjacent to the nitrogen atoms), indicating a coplanar orientation of the aromatic planes of the guest with respect to the cavity sidewalls. This host-guest binding geometry is in line with that observed in the X-ray structure of the related ternary complex **^{113}Cd1**−**$(MCy)_2V$**−**MeCN** (*vide infra*, Figure 6E).

Kinetic allosteric effects

Typically, cooperativity effects in host-guest systems are expressed in the thermodynamics of binding. In the following we will also discuss kinetic aspects of the allosteric system based on **Cd1**, i.e., to what extent the dissociation rate of a bound **Me_2V** guest is influenced by the presence of a coordinating **tbupy** ligand. Previously, kinetic cooperativity has been described for natural systems, e.g. for changes in substrate conversion rates by enzymes.[24] We investigated the kinetic factors of the allosteric effect of the binding in **Cd1** with the help of 1D Exchange Spectroscopy (EXSY) NMR experiments.[25]

These experiments require the exchange process to be slow on the chemical shift timescale, i.e., individual signals must be present for both the free and bound states, not coalesced. This condition was satisfied for the complex of **Cd1** with **Me_2V** but not for the complex of **Cd1** with **DMI**. The coordination of a **tbupy** ligand to **Cd1**−**Me_2V** at the outside of the cage led to a decrease in the exchange rate of the host-guest complex with **Me_2V**, which is visible from a sharpening of the guest signals in the NMR spectra. Similarly, binding of **tbupy** to **Cd1**−**DMI** decreases the exchange rate of **DMI**, which was apparent from the broadening of the **DMI** signal due to a transition from the fast to intermediate exchange regime; however, the exchange rate was not reduced sufficiently to permit 1D EXSY measurements.[23] By extrapolating the dissociation rate constants from Eyring plots (Figure 4) of **Cd1**−**Me_2V** and **tbupy-Cd1**−**Me_2V**, it was observed that the presence of **tbupy** results in a ~25-fold decrease in dissociation rate ($k_{-1,298K}$ = 64.4 s^{-1} vs $^{tbupy}k_{-1,298K}$ = 2.59 s^{-1}), respectively.

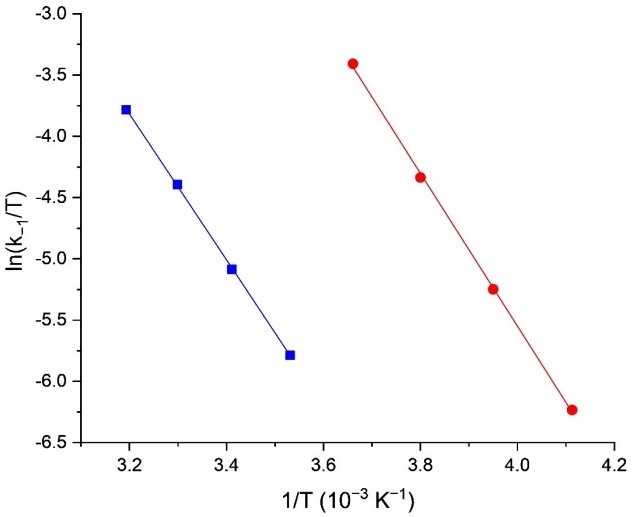

Figure 4. Eyring plots of the dissociation of **Me_2V** from **Cd1** in the presence (blue) and the absence (red) of **tbupy**. [**Cd1**] = 0.849 mM, [**Me_2V**] = 1.86 mM and [**tbupy**] = 0 or 44.3 mM in $CDCl_3/CD_3CN$ (1 : 1, v/v).

This kinetic allosteric effect had not been quantified for complexes of porphyrin cages with low molecular weight guests before, but it has been established for complexes of polymer-appended viologen derivatives with **Zn1**.[3] A comparison of the activation enthalpy and entropy values derived from the Eyring plots indicates that the difference in dissociation rates is caused by only a slight difference in enthalpy, but a significant difference in the entropy of the exchange process (Table 3).

The negative activation entropies are likely associated with the solvation of **Me_2V** once it exits the cavity.[25] Prior to **Me_2V** dissociation, **Cd1** in the absence of **tbupy** likely has an acetonitrile bound. We propose that after guest dissociation, this outside acetonitrile molecule is replaced by an acetonitrile molecule that coordinates on the inside of the cage, thereby solvating it to some extent. In the presence of **tbupy**, the activation entropy for **Me_2V** dissociation is more negative, which we attribute to a difference in solvation of **Cd1** after dissociation of the guest. Both prior to and after **Me_2V** dissociation, the **tbupy** ligand remains coordinated to the cadmium center at the outside of the cage of **Cd1**. After dissociation of **Me_2V**, the empty cage cannot be solvated via the coordination of an acetonitrile molecule to the already penta-coordinate cadmium center. The cavity will then be filled sub-optimally with multiple non-coordinating solvent mole-

Table 3. Activation energy parameters (T = 298 K) associated with the dissociation of **Me_2V** (*c* = 1.86 mM) from the cavity of **Cd1** (*c* = 0.85 mM) in the absence and presence of a coordinated **tbupy** ligand, in $CDCl_3/CD_3CN$ (1 : 1, (v/v)

[**tbupy**] [mM]	$\Delta H^{\neq}$ (kJ·mol^{-1})	$\Delta^{\neq}$ (J·K^{-1}·mol^{-1})	$\Delta G^{\neq}$ (kJ·mol^{-1})
0	53.09 ± 0.96	−31.69 ± 0.67	62.55 ± 0.96
44.3	49.45 ± 0.50	−71.22 ± 0.75	70.67 ± 0.46

Research Article
doi.org/10.1002/ejoc.202200111

cules, resulting in an entropically disfavored effect on the dissociation (Figure 5). In addition, due to its weaker coordination as a result of **Me_2V** dissociation, partial dissociation of **tbupy** from **Cd1**, and the subsequent solvation of this ligand and the porphyrin may also contribute to the more negative activation entropy.

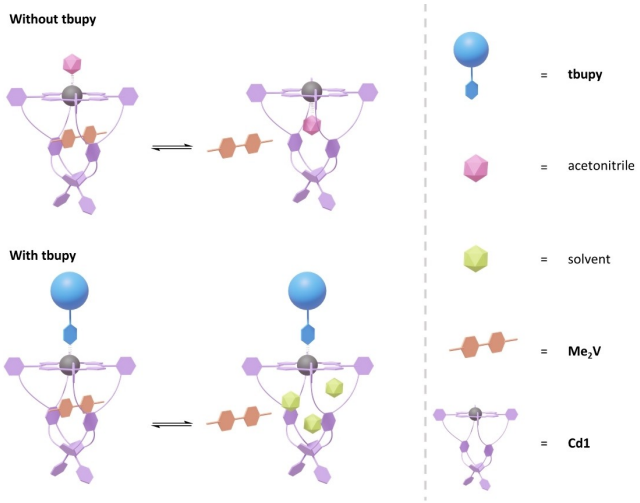

Figure 5. Proposed differences in solvation of **Cd1** post and prior **Me_2V** dissociation in the presence and absence of **tbupy**.

Crystal structures

Several single crystals of **Cd1** and its complexes could be obtained, and the corresponding crystal structures were solved by X-ray crystallography (Figure 6). In these structures, the overall geometry of the cage framework of **Cd1** remains largely the same, and the most pronounced difference is the position of the cadmium center coordinated to the porphyrin (Table 4).

In Figure 6A, the crystal structure of **Cd1** with an axially coordinated acetone molecule is shown (CCDC 2144871). This ligand, which resides in the cavity of the cage, pulls the cadmium center out of the porphyrin plane by 0.657 Å. In Figure 6B, the crystal structure of **Cd1** with an axially coordinated acetonitrile molecule inside the cavity is shown (CCDC 2144873), where the cadmium center is pulled out of the porphyrin plane by 0.798 Å. The difference in distance that the cadmium center is pulled out of the porphyrin plane is likely caused by the formation of hydrogen bonds between the methyl groups of the ligands and the urea carbonyl groups, which requires some slight reorganization of the cadmium

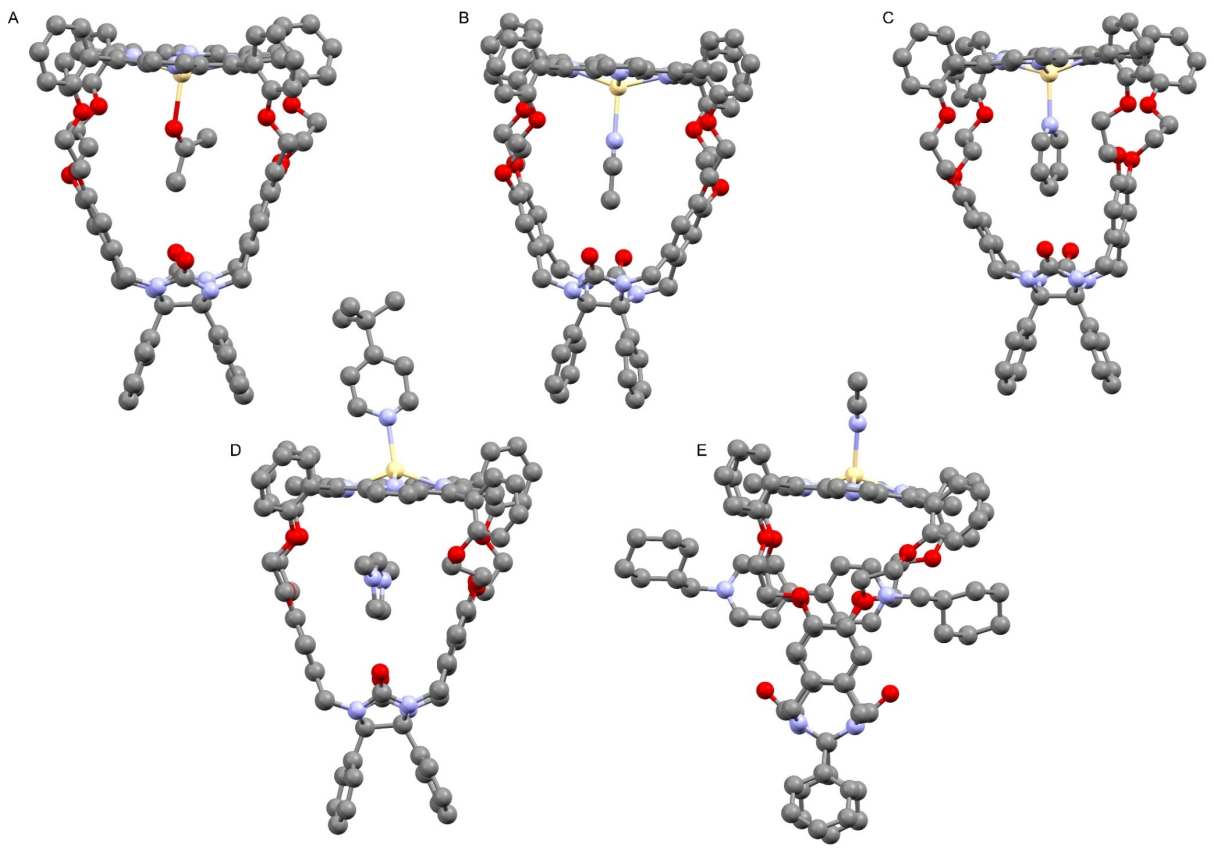

Figure 6. Crystal structures of (A) **Cd1** with an axially coordinated acetone molecule (CCDC number 2144871), (B) **Cd1** with an axially coordinated acetonitrile molecule (CCDC number 2144873), (C) **Cd1** with an axially coordinated **py** molecule (CCDC number 2144872), (D) **Cd1** with a bound **DMI** guest and an axially coordinated **tbupy** molecule (CCDC number 2144874), and (E) **Cd1** with a bound **$(MCy)_2V$** guest and an axially coordinated acetonitrile molecule (CCDC number 2145163). Non-coordinating solvent molecules, counter ions and hydrogen atoms have been omitted for clarity.

Research Article
doi.org/10.1002/ejoc.202200111

Table 4. Selected distances in the crystal structures of **Cd1** complexed with various ligands/guests. 24 mp = mean plane through the 24 carbon/nitrogen atoms of the porphyrin; CO = urea carbonyl groups.

Complex	Cd – 24 mp [Å][a]	CO – 24 mp [Å][b]		C-30 – C-30 [Å][c]	
Cd1-acetone	0.657	8.379	8.353	6.911	6.633
Cd1–MeCN	0.798	8.219	8.219	6.842	6.842
Cd1-**py**	0.695	8.639	8.460	6.591	6.383
Cd1–**DMI**-**tbupy**	0.790	8.196	7.776	6.516	6.445
Cd1–**$(MCy)_2V$**–MeCN	0.690	8.827	8.433	5.947	6.024

[a] Displacement of the Cd-center perpendicular to the mean porphyrin plane. [b] The two distances between the mean plane and the urea carbonyl oxygen atoms. [c] The two istances between carbon atoms C-30 at the aromatic rings of the two cavity portals.

center to allow for the most favorable bond angles and distances. The distance between the hydrogen atoms of the ligand and these urea carbonyl groups is 2.89 Å for acetone and 2.82 Å for acetonitrile with respective CH···O bond angles of 128.1° and 146.0°. The methyl groups of the ligands in these complexes are in close proximity to the aromatic rings of the cavity sidewalls of **Cd1** (3.01 Å and 3.03 Å for acetone, and 2.79 Å and 3.28 Å for acetonitrile between the CH_3-protons and the centers of the sidewalls), indicating the presence of CH···π interactions between the host and the ligands. In the crystal structure of **Cd1** with a coordinated pyridine molecule inside the cavity (CCDC 2144872), the ligand pulls the cadmium center out of the plane by 0.695 Å (Figure 6C). The **py** ligand inside the cavity of **Cd1** pulls the metal center significantly further out of the porphyrin plane than in the analogous crystal structure of the complex of this ligand with **Zn1** (0.359 Å),[3] while the remainder of the two crystal structures is almost identical. Figure 6D shows the crystal structure of **Cd1** with a **DMI** guest bound in its cavity and a **tbupy** ligand coordinated to the metal center on the outside of the cage (CCDC 2144874). Here, the cadmium center is displaced 0.790 Å outwards of the porphyrin plane in the direction of the **tbupy** ligand. The displacements of the cadmium center from the mean porphyrin plane in the crystal structures are in line with those observed for previously reported cadmium porphyrin complexes with axial ligands such as 1,4-diazabicyclo[2.2.2]octane (DABCO) (0.746 Å)[26] and morpholine (0.60 Å).[27] The displacements are not the result of a too-tight fit of the cadmium center, since in the crystal structure of a cadmium porphyrin with two dioxane axial ligands, the cadmium center is located in the porphyrin plane.[17]

Multiple attempts to grow single crystals of the **Me_2V**–**Cd1** complex failed, but the crystal structure of **Cd1** with a viologen guest with different *N*-substituents, i.e. *N*,*N*′-bis(cyclohexylmethyl)viologen dihexafluorophosphate **$(MCy)_2V$** (see Figure 1), could be successfully solved (Figure 6E) (CCDC 2145163). Interestingly, the viologen guest bound in the cavity is not centered. The positively charged nitrogen atom of one of the pyridinium rings is positioned closely to the oxygen atoms of the ethyleneoxy linkers of the cage, while the other pyridinium ring is located slightly outside the cage. The axially coordinated acetonitrile molecule pulls the cadmium center out of the porphyrin plane by 0.690 Å. In the X-ray structure of the ternary allosteric complex of **Cd1** with **DMI** and **tbupy** (Figure 6D), the imidazolium ring of **DMI** is oriented in a coplanar fashion with respect to the cavity sidewalls of **Cd1**, which is in agreement with shifts observed in the ^{1}H NMR spectra of this host-guest complex. Furthermore, the imidazolium 4,5-protons are at a (weak) hydrogen bonding distance of 2.323 and 2.803 Å from the urea carbonyl groups of the host, at CH···O bond angles of 165.6 and 167.9°, respectively.

In addition to the variations in the displacement of the Cd center from the porphyrin, we also compared the effects of coordinated ligands and bound guests on cavity size and shape of **Cd1** in the X-ray structures (Table 4). A comparison of the distances between the mean porphyrin plane and the urea carbonyl groups ("cavity height") did not reveal a clear trend. A comparison between the distances of the xylylene side-walls ("cavity width") showed that the coordination of the methyl-containing axial ligands (acetone and acetonitrile) widened the cavity, whereas the binding of the **Cd1**–**$(MCy)_2V$** guest caused a narrowing. However, it is not straightforward to use these differences in drawing conclusions with regard to geometric aspects of the allosteric effect, since variations in bulkiness of the guests and ligands inside the confined cavity will each have their own impact on cavity size and shape as well.

Conclusion

A ternary host-guest-ligand system comprised of **Cd1**, **DMI**, and **tbupy** displays allosteric behavior, in which the coordination of **tbupy** to the outside of the cage of **Cd1** leads to a 31-fold increase in binding strength of **DMI** inside the cavity of the host. Vice versa, the binding of **DMI** leads to a 55-fold increase in the binding strength of the **tbupy** ligand. The crystal structure of the allosteric complex has been solved, and it shows that the **tbupy** ligand pulls the cadmium metal center out of the porphyrin plane by 0.790 Å. This metal relocation is probably an important driving force for the enhanced binding of the guest (either **DMI** or **Me_2V**) inside the cavity of **Cd1**: the cavity is sterically more available for the binding of the guest, and there is less electrostatic repulsion between the metal center and the cationic charge(s) of the guest. Similarly, the binding of **DMI** or **Me_2V** in the cavity of **Cd1** is believed to relocate the cadmium center to the outside of the cage, thereby exposing it to the coordination of an axial ligand. The ^{113}Cd signal in ^{113}Cd NMR spectra can be used as an antenna for quantifying the binding of axial ligands, such as **tbupy** and acetonitrile, whose coordinations only display a marginal effect in the ^{1}H NMR spectra. In addition to thermodynamic allostery, host **Cd1** also displays kinetic allostery. The dissociation rate of **Me_2V** from the cavity of **Cd1** is reduced 25-fold in the presence of a **tbupy** ligand coordinating to the Cd center at the outside of the cage. Regardless of the presence of the axial ligand, the enthalpy of activation of dissociation of **Me_2V** from **Cd1** remains largely the same, while the entropy of activation becomes less favorable by 39.5 $J \cdot K^{-1} \cdot mol^{-1}$ when the ligand is present. These findings indicate that the kinetic allosteric effect is entropic in nature.

Experimental Section

General information

Acetonitrile was distilled from calcium hydride and chloroform from Sicapent under a nitrogen atmosphere. Other solvents and reagents were obtained from commercial suppliers and used without further purification. Reactions were monitored using thin-layer chromatography (TLC) on silica gel-coated plates (Merck 60 F254). Detection was performed with UV light at 254 nm. Column chromatography was performed manually using Acros silica gel, 0.035–0.070 mm, 60 A, which was deacidified by stirring for 24 h in methanol with one mass percent of K_2CO_3 followed by evaporation of the methanol. NMR spectra were recorded at 298 K on a Bruker Avance III 500 spectrometer equipped with a Prodigy BB cryoprobe. ^{1}H NMR and ^{13}C NMR chemical shifts (δ) are given in parts per million (ppm) and were referenced to tetramethylsilane (0.00 ppm). The frequencies for the other spectra were referenced to the frequency of the ^{1}H NMR spectra. Coupling constants are reported as *J* values in Hertz (Hz). Data for the ^{1}H NMR spectra are reported as follows: chemical shift (multiplicity, coupling constant, integration). Multiplicities are abbreviated as s (singlet), d (doublet), t (triplet), m (multiplet), b (broad). Mass spectra were recorded on an JEOL AccuTOF CS JMS-T100CS mass spectrometer or on a Bruker Microflex LRF MALDI-TOF system in reflective mode, employing dithranol as a matrix. The reflections of single crystals were measured on a Bruker D8 Quest diffractometer with sealed tube and Triumph monochromator (λ = 0.71073 Å). The software package used for the intensity integration was Saint (v8.40a).[28] Absorption correction was performed with SADABS.[29] The structures were solved with direct methods using SHELXT-2014/5.[30] Least-squares refinement was performed with SHELXL-2018/3[31] against of $\left|F_h^o\right|^2$ all reflections. Non-hydrogen atoms were refined freely with anisotropic displacement parameters. Hydrogen atoms were placed on calculated positions or located in difference Fourier maps. All calculated hydrogen atoms were refined with a riding model. UV-vis spectra were recorded on a JASCO V-630 or on a Varian Cary 50 UV-Vis spectrophotometer. The baseline was always recorded in the same solvent and in the same cell as the samples. The spectra are presented without smoothing and further data processing.

General procedure for titrations

UV-vis titrations were performed by preparing a ~0.2 mM stock solution of **Cd1** in a deoxygenated 1:1 v/v mixture of $CHCl_3$/MeCN or $CHCl_3$. From these stock solutions the titration sample solutions were prepared with identical **Cd1** and optional additive concentrations, 2.0 μM (for **DMI** titrations) or 0.5 μM (for **Me_2V** titration), to prevent dilution during the experiment. To a solution containing no guest/ligand, a solution containing the guest/ligand was added in small quantities, and after each addition a UV-vis spectrum was recorded to provide the data presented in Tables S5.40–S5.67. The combined data at multiple wavelengths was fitted using an online fitting tool: http://app.supramolecular.org/bindfit/[32,33] to provide the association constants and fits shown in Table 1 and S5.1. NMR titrations were performed analogously by adding a solution of the appropriate guest/ligand with the host to a solution with the host (to account for dilution) in deuterated solvents followed by the recording of a spectrum. **Cd1** concentrations varied from 0.65 to 0.91 mM. The combination of various shifting signals was fitted using the same online fitting tool: http://app.supramolecular.org/bindfit/[32,33] to provide the fits shown in Tables S5.2–S5.39 and association constants shown in Table 1 and S5.1. ^{113}Cd titrations were performed by indirectly measuring the ^{113}Cd signal via an ^{1}H-^{113}Cd HMBC spectrum due to the time that would be required for performing direct ^{113}Cd measurements (order of minutes vs order of hours).

General procedure for exchange experiments

All exchange experiments were performed on a Bruker 500 MHz Avance III spectrometer equipped with a Prodigy BB cryoprobe. For each experiment, four different temperature points were used for the exchange measurements. The temperature range was selected per sample such that a suitable mix time range could be obtained. For slower exchanging systems, higher temperatures (10 °C to 40 °C) were selected, and for faster exchanging systems, lower temperatures (−30 °C to 0 °C) were used. Prior to each exchange measurement, the temperature of the probe was calibrated using pure ethylene glycol for temperatures ≥20 °C and methanol for temperatures <20 °C. Afterwards, the probe was tuned and shimmed, and the 90° pulse and the T_1 for the methyl protons of bound **Me_2V** were measured for the sample at each temperature point. Then, 8 data points were set up as 1D NOESY experiments irradiated at the frequency of the methyl protons of bound **Me_2V** at different mix times, followed by the recording of a quantitative ^{1}H NMR spectrum. For every temperature point, a quantitative proton spectrum was measured to ensure that the concentration of the sample stayed the same over time.

General procedure for cadmium insertion

$Cd(OAc)_2 \cdot 2\ H_2O$ or $^{113}Cd(OAc)_2 \cdot 2\ H_2O$ and K_2CO_3 were added to a solution of **H_2TPP** or **$H_2$1** in a 1:2 (v/v) MeOH/$CHCl_3$ mixture (1.0 mM) and the mixture was stirred at reflux temperature for 16 h. The mixture was cooled to room temperature, concentrated, diluted with $CHCl_3$ (100 mL), and washed with H_2O three times. The organic layer was concentrated, and the product was purified by silica gel flash column chromatography (de-acidified 60 A silica gel, eluent 5% (v/v) MeCN/$CHCl_3$). The product was precipitated from dichloromethane/*n*-heptane and washed with *n*-pentane to give the products as green powders.

CdTPP was obtained from **H_2TPP** (418 mg, 680 μmol), K_2CO_3 (729 mg, 5.27 mmol) and $Cd(OAc)_2 \cdot 2\ H_2O$ (548 mg, 2.06 mmol) in 67% yield (328 mg, 452 μmol). ^{1}H NMR (500 MHz, $CDCl_3$) δ 8.82 (m, $^4J_{1H-113Cd}$ = 5.2 Hz, 8H, β-pyrrole), 8.22 (d, *J* = 6.6 Hz, 8H, *H*-22, *H*-26), 7.81–7.72 (m, 12H, *H*-23, *H*-24, *H*-25). ^{13}C NMR (126 MHz, $CDCl_3$) δ 150.66, 136.76 (*C*-22), 132.24 (β-pyrrole), 127.31 (*C*-23 or *C*-24), 126.42 (*C*-23 or *C*-24). HRMS (ESI-TOF) (*m/z*): $[M+H]^+$ calcd. for $C_{44}H_{29}{}^{110}CdN_4$, 723.14223; found, 723.14460.[16]

Cd1 was obtained from **$H_2$1** (100 mg, 74.3 μmol), K_2CO_3 (100 mg, 724 μmol) and $Cd(OAc)_2 \cdot 2\ H_2O$ (80 mg, 0.30 mmol) in 90% yield (105 mg, 72 μmol). (NMR spectra (*c* = 2.0 mM)) **^{1}H NMR** (500 MHz, $CDCl_3$) δ 8.81 (m, $^4J_{1H-113Cd}$ = 5.4 Hz, 4H, *H-3,4,13,14*), 8.64 (m, $^4J_{1H-113Cd}$ = 5.9 Hz, 4H, *H-8,9,18,19*), 8.08 (dd, *J* = 7.3, 1.8 Hz, 4H, *H-22*), 7.74 (td, *J* = 7.8, 1.8 Hz, 4H, *H-24*), 7.40–7.31 (m, 8H, *H-23,25*), 6.99–6.90 (m, 6H, *H-39-41,45-47*), 6.73–6.67 (m, 4H, *H-38,42,44,48*), 6.06 (s, 4H, *H-30*), 4.21 (ddd, *J* = 11.0, 7.7, 3.5 Hz, 4H, *H-27b*), 4.06–3.95 (m, 8H, *H-27a,32a*), 3.61 (d, *J* = 15.8 Hz, 4H, *H-32b*), 3.48 (dt, *J* = 10.4, 4.2 Hz, 4H, *H-28b*), 3.26 (ddd, *J* = 10.7, 7.7, 3.5 Hz, 4H, *H-28a*). ^{13}C NMR (126 MHz, $CDCl_3$) δ 159.00 (*C-26*), 156.86 (*C-33,34*), 150.43 (*C-2,5,12,15*), 150.20 (*C-7,10,17,20*), 146.59 (*C-29*), 135.90 (*C-22*), 133.55 (*C-37,43*), 133.09 (*C-21*), 131.58 (*C-3,4,13,14*), 131.21 (*C-8,9,18,19*), 129.83 (*C-31*), 129.23 (*C-24*), 128.53 (*C-40,46*), 128.50 (*C-39,41,45,47*), 128.07 (*C-38,42,44,48*), 119.74 (*C-23*), 116.54 (*C-1,6,11,16*), 115.33 (*C-30*), 112.10 (*C-25*), 84.66 (*C-35,36*), 67.67 (*C-28*), 67.12 (*C-27*), 44.20 (*C-32*). HRMS (ESI-TOF) (*m/z*): $[M+H]^+$ calcd. for $C_{84}H_{63}CdN_8O_{10}$, 1455.3717; found, 1455.3857 (overlay of calculated and measured data in S3.1). UV-vis ($CHCl_3$) λ_{max}, nm (ε): 432 (2.13×10^5 L·mol^{-1}·cm^{-1}), 566 (1.67×10^4 L·mol^{-1}·cm^{-1}), 605 ($6.81 \times$

10^3 L·mol^{-1}·cm^{-1}). UV-vis ($CHCl_3$/MeCN (1:1 v/v)) λ_{max}, nm (ε): 434 (3.67×10^5 L·mol^{-1}·cm^{-1}), 572 (1.58×10^4 L·mol^{-1}·cm^{-1}), 609 (8.47×10^3 L·mol^{-1}·cm^{-1}). Melting point >300 °C.

^{113}Cd1 was obtained from **$H_2$1** (130 mg, 96.6 μmol), K_2CO_3 (105 mg, 760 μmol) and $^{113}Cd(OAc)_2\cdot2\ H_2O$ (57 mg, 0.21 mmol) in 81% yield (114 mg, 78 μmol). (NMR spectra (c=1.0 mM)) ^{1}H NMR (500 MHz, $CDCl_3$) δ 8.82 (m, $^4J_{1H-113Cd}$=5.9 Hz, 4H, *H-3,4,13,14*), 8.64 (m, bk; $^4J_{1H-113Cd}$=6.3 Hz, 4H, *H-8,9,18,19*), 8.09 (dd, J=7.3, 1.7 Hz, 4H, *H-22*), 7.74 (ddd, J=8.4, 7.6, 1.8 Hz, 4H, *H-24*), 7.39–7.31 (m, 8H, *H-23,25*), 6.99–6.91 (m, 6H, *H-39-41,45-47*), 6.77–6.69 (m, 4H, *H-38,42,44,48*), 6.11 (s, 4H, *H-30*), 4.23 (ddd, J=11.0, 7.8, 3.5 Hz, 4H, *H-27b*), 4.11–4.02 (m, 8H, *H-27a,32a*), 3.66 (d, J=15.8 Hz, 4H, *H-32b*), 3.51 (ddd, J=10.4, 4.8, 3.5 Hz, 4H, *H-28b*), 3.29 (ddd, J=10.8, 7.7, 3.4 Hz, 4H, *H-28a*). ^{13}C NMR (126 MHz, $CDCl_3$) δ 158.99 (*C-26*), 156.90 (*C-33,34*), 150.39 (*C-2,5,12,15*), 150.16 (*C-7,10,17,20*), 146.60 (*C-29*), 135.92 (*C-22*), 133.49 (*C-37,43*), 133.06 (*C-21*), 131.62 (d, J=14.5 Hz, *C-3,4,13,14*), 131.26 (d, J=14.5 Hz, *C-8,9,18,19*), 129.88 (*C-31*), 129.24 (*C-24*), 128.53 (*C-40,46*), 128.48 (*C-39,41,45,47*), 128.09 (*C-38,42,44,48*), 119.73 (*C-23*), 116.61 (*C-1,6,11,16*), 115.29 (*C-30*), 112.04 (*C-25*), 84.69 (*C-35,36*), 67.66 (*C-28*), 67.10 (*C-27*), 44.26 (*C-32*). ^{113}Cd NMR (111 MHz, $CDCl_3$) δ −174.37.

Crystallographic data

Deposition numbers 2144871 (for **Cd1**-acetone), 2144873 (for **Cd1**-MeCN), 2144872 (for **Cd1**-**py**), 2144874 (for **Cd1**-**DMI**-**tbupy**), and 2145163 (for **Cd1**-**(MCy)$_2$V**-MeCN) contain the supplementary crystallographic data for this paper. These data are provided free of charge by the joint Cambridge Crystallographic Data Centre and Fachinformationszentrum Karlsruhe Access Structures service www.ccdc.cam.ac.uk/structures.

Acknowledgements

This work was supported by the European Research Council (ERC Advanced Grant 740295 ENCOPOL to R.J.M.N.) and a grant from the Dutch Ministry of Education, Culture and Science (Gravitation Program 024.001.035).

Conflict of Interest

The authors declare no conflict of interest.

Data Availability Statement

The data that support the findings of this study are available from the corresponding author upon reasonable request.

Keywords: Allostery · Host-guest chemistry · Cadmium · Porphyrin · Cooperativity

[1] J. A. A. W. Elemans, R. J. M. Nolte, *Chem. Commun.* **2019**, *55*, 9590–9605.
[2] M. G. T. A. Rutten, F. W. Vaandrager, J. A. A. W. Elemans, R. J. M. Nolte, *Nat. Chem. Rev.* **2018**, *2*, 365–381.
[3] A. B. C. Deutman, C. Monnereau, M. Moalin, R. G. E. Coumans, N. Veling, M. Coenen, J. M. M. Smits, R. de Gelder, J. A. A. W. Elemans, G. Ercolani, R. J. M. Nolte, A. E. Rowan, *Proc. Natl. Acad. Sci. USA* **2009**, *106*, 10471–10476.
[4] J. A. A. W. Elemans, E. J. A. Bijsterveld, A. E. Rowan, R. J. M. Nolte, *Eur. J. Org. Chem.* **2007**, 751–757.
[5] P. Thordarson, E. J. A. Bijsterveld, A. E. Rowan, R. J. M. Nolte, *Nature* **2003**, *424*, 915–918.
[6] P. J. Thomassen, S. Varghese, E. J. A. Bijsterveld, P. Thordarson, J. A. A. W. Elemans, A. E. Rowan, R. J. M. Nolte, *Eur. J. Org. Chem.* **2015**, 5246–5253.
[7] P. Thordarson, R. G. E. Coumans, J. A. A. W. Elemans, P. J. Thomassen, J. Visser, A. E. Rowan, R. J. M. Nolte, *Angew. Chem. Int. Ed.* **2004**, *43*, 4755–4759; *Angew. Chem.* **2004**, *116*, 4859–4863.
[8] P. Thordarson, E. J. A. Bijsterveld, J. A. A. W. Elemans, P. Kasák, R. J. M. Nolte, A. E. Rowan, *J. Am. Chem. Soc.* **2003**, *125*, 1186–1187.
[9] J. P. J. Bruekers, M. A. Hellinghuizen, N. Vanthuyne, P. Tinnemans, P. J. Gilissen, W. J. Buma, J.-V. Naubron, J. Crassous, J. A. A. W. Elemans, R. J. M. Nolte, *Eur. J. Org. Chem.* **2021**, 607–617.
[10] S. Cantekin, A. J. Markvoort, J. A. A. W. Elemans, A. E. Rowan, R. J. M. Nolte, *J. Am. Chem. Soc.* **2015**, *137*, 3915–3923.
[11] I. M. Armitage, R. T. Pajer, *J. Am. Chem. Soc.* **1976**, *98*, 5710–5712.
[12] D. B. Bailey, P. D. Ellis, J. A. Fee, *Biochemistry* **1980**, *19*, 591–596.
[13] A. R. Palmer, D. B. Bailey, W. D. Benhke, A. D. Cardin, P. P. Yang, P. D. Ellis, *Biochemistry* **1980**, *19*, 5063–5070.
[14] K. McAteer, A. S. Lipton, M. A. Kennedy, P. D. Ellis, *Solid State Nucl. Magn. Reson.* **1996**, *7*, 229–238.
[15] F. Jalilehvand, B. O. Leung, V. Mah, *Inorg. Chem.* **2009**, *48*, 5758–5771.
[16] H. J. Jakobsen, P. D. Ellis, R. R. Inners, C. F. Jensen, *J. Am. Chem. Soc.* **1982**, *104*, 7442–7452.
[17] P. F. Rodesiler, E. H. Griffith, P. D. Ellis, E. L. Amma, *J. Chem. Soc. Chem. Commun.* **1980**, 492–493.
[18] P. D. Ellis, R. R. Inners, H. J. Jakobsen, *J. Phys. Chem.* **1982**, *86*, 1506–1508.
[19] S. Le Gac, L. Fusaro, V. Dorcet, B. Boitrel, *Chem. Eur. J.* **2013**, *19*, 13376–13386.
[20] P. Patnaik, *Handbook of Inorganic Chemicals*, First edition, McGraw-Hill, United States of America **2002**, 143–144.
[21] J. N. H. Reek, A. H. Priem, H. Engelkamp, A. E. Rowan, J. A. A. W. Elemans, R. J. M. Nolte, *J. Am. Chem. Soc.* **1997**, *119*, 9956–9964.
[22] P. D. Ellis, *Science* **1983**, *221*, 1141–1146.
[23] T. D. W. Claridge, *High-Resolution NMR Techniques in Organic Chemistry*, third edition, Elsevier Netherlands, **2016**, Ch. 2.
[24] C. M. Porter, B. G. Miller, *Bioorg. Chem.* **2012**, *43*, 44–50.
[25] A. Swartjes, P. B. White, M. Lammertink, J. A. A. W. Elemans, R. J. M. Nolte, *Angew. Chem. Int. Ed.* **2021**, *60*, 1254–1262; *Angew. Chem.* **2021**, *133*, 1274–1282.
[26] C. Mchiri, A. Ouakouak, S. Nasri, A. Jedidi, I. Turowska-Tyrk, S. Acherar, C. Frochot, T. Roisnel, H. Nasri, *Inorg. Chim. Acta.* **2021**, *515*, 120046.
[27] C. Mchiri, S. Dhifaoui, K. Ezzayani, M. Guergueb, T. Roisnel, F. Loiseau, H. Nasri, *Polyhedron* **2019**, *171*, 10–19.
[28] SAINT V8.38 A. Bruker AXS Inc., Madison, Wisconsin, USA.
[29] SADABS-2016/2, L. Krause, R. Herbst-Irmer, G. M. Sheldrick, D. J. Stalke, *J. Appl. Crystallogr.* **2015**, *48*, 3–10.
[30] G. M. Sheldrick, *J. Appl. Crystallogr.* **2015**, A*71*, 3–8.
[31] G. M. Sheldrick, *J. Appl. Crystallogr.* **2015**, C*71*, 3–8.
[32] D. B. Hibbert, P. Thordarson, *Chem. Commun.* **2016**, *52*, 12792–12805.
[33] http://supramolecular.org/.

Manuscript received: February 4, 2022
Revised manuscript received: March 22, 2022